Int. J. Solids Structures Vol. 22, No. 12, pp. 1599–1627, 1986
Printed in Great Britain.

0020-7683/86 $3.00+.00
Pergamon Journals Ltd.

FRAME ANALYSIS WITH PANEL ZONE DEFORMATION

ERIC M. LUI†
Department of Civil Engineering, Syracuse University, Syracuse, NY 13244, U.S.A.

AND

WAI-FAH CHEN‡
Department of Structural Engineering, School of Civil Engineering, Purdue University, West Lafayette, IN 47907, U.S.A.

(*Received* 4 *June* 1985; *in revised form* 28 *February* 1986)

Abstract—Conventional analyses of frameworks are usually carried out without considering the effect of panel zone deformation on frame behavior. As a result, center-to-center distances rather than clear spans are used for the lengths of the members. As is evident from experimental studies, the effect of panel zone deformation has a pronounced influence on frame behavior. In particular, the strength and drift of the frame will be affected if panel zone deformation is taken into consideration in the analysis. In this paper, various deformation modes of the panel zone are identified. A simple model which can be used to represent all these modes is then presented. The validity of this model is established by comparison with experiments on joint subassemblages. Finally, a two-bar frame with different behavioral joint models is analyzed numerically to demonstrate the importance of using realistic models in frame analysis.

INTRODUCTION

In a steel frame, if the beam is framed into the flange of the column, there exists a region called the panel zone which is composed of the web and flanges of the column (Fig. 1). The behavior of this panel zone has a significant influence on the behavior of the frame. Figure 2 shows a possible system of forces that acts on the joint panel of an interior beam-to-column connection. Under the action of these forces, the joint panel will deform. The various deformation modes are shown in Fig. 3. In addition to causing deformation, these forces may cause premature yielding of the panel zone resulting in a reduction in strength and stiffness of the frame.

Numerous tests[1, 2, 4–7] have been performed in the past decade to investigate the load–deformation behavior of the joint panel using connection subassemblages. Particular attention was given to the shear capacity of the panel zone and the effect of panel zone shear deformation on the strength and stiffness of the subassemblages. The significant features observed in these tests are:

1. There are two distinct stiffnesses in the joint shear force-determination response of the panel. An elastic stiffness, followed by a smaller, almost constant stiffness for a long range of deformation (Fig. 4).
2. Large ductility of the joint panel is observed before failure.
3. Failure is usually caused by fracture of the welds or beam flange on the face of the column flange.

The existence of a second or post yield stiffness in the shear force–deformation response is attributed to the following:

1. The resistance of the boundary elements such as the column flanges and stiffeners of the joint panel.
2. The onset of strain-hardening of the web of the joint panel before complete yielding of the boundary elements.
3. The restraint from the adjoining beams and columns.

† Assistant Professor.
‡ Professor and Head of Department.

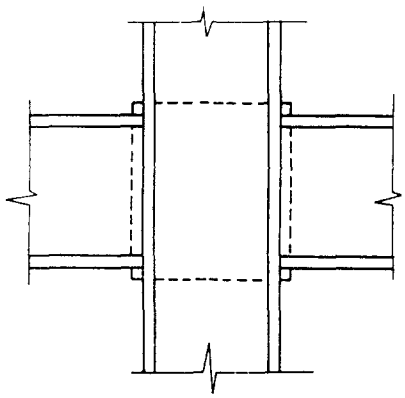

Fig. 1. Panel zone.

Based on these observations, a finite element model of the panel zone is presented. This model is capable of representing the various modes of deformation depicted in Fig. 3. In addition, yielding and strain-hardening of the web panel are considered. The validity of this model will be demonstrated by comparison with experiments.

BASIC ASSUMPTIONS

The assumptions used for the model are:

1. An elastic–perfectly plastic strain-hardening stress–strain behavior of the web panel is assumed (Fig. 5).
2. Although large rigid body rotation of the joint panel is allowed, the deformation or distortion of the point panel remains small.
3. No local buckling or lateral torsional buckling of the panel is allowed. In other words, only strength limit state will be considered for the joint panel in the model.
4. Yielding of the web of the joint panel will occur as the state of stress reaches the yield surface described by the Von Mises or J_2 theory.
5. Isotropic hardening rule is used to describe the subsequent yield or loading surfaces.
6. Fracture of the material is not considered.

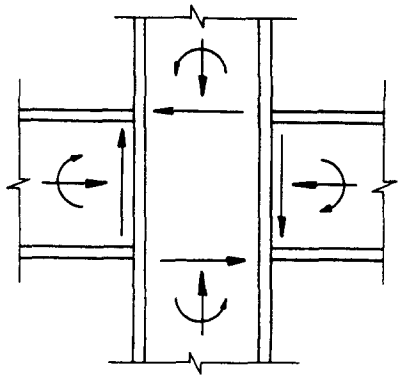

Fig. 2. Forces acting on a panel zone.

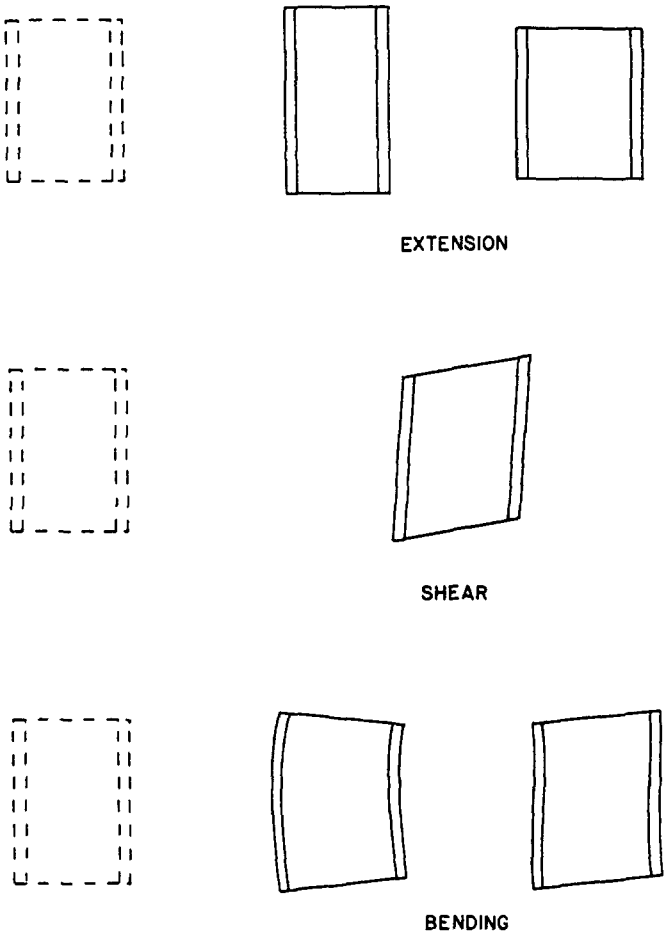

Fig. 3. Deformation modes of a joint panel.

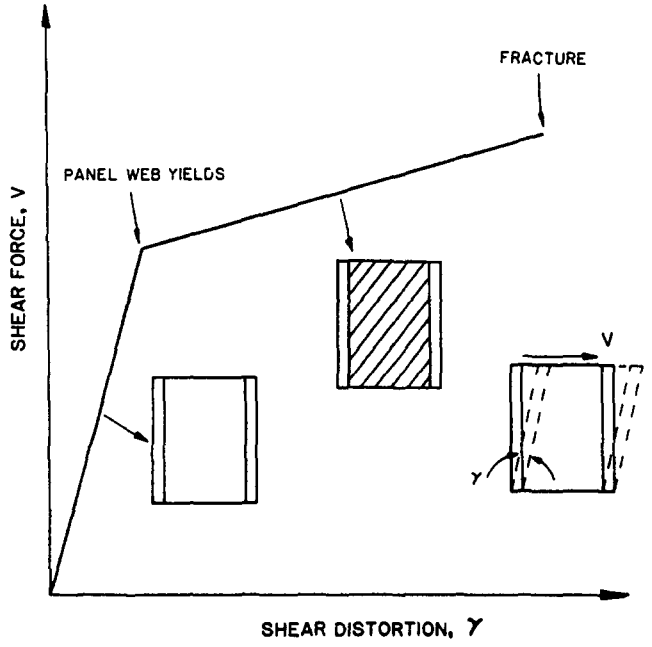

Fig. 4. Typical shear force–distortion behavior of a joint panel.

Finite element model of panel zone

The finite element model of the panel zone is shown in Fig. 6. It consists of three elements: one web element and two flange elements. The local (ξ, η) coordinate systems and degrees of freedom of these elements are shown in Fig. 6.

Web panel. Refer to Fig. 6(b), the assumed displacement field for this element is

$$\begin{pmatrix} u \\ v \\ \theta \end{pmatrix} = \begin{pmatrix} u(\xi, \eta) \\ v(\xi, \eta) \\ -\dfrac{\partial u(\xi, \eta)}{\partial y} \end{pmatrix}$$

or

$$\begin{pmatrix} u \\ v \\ \theta \end{pmatrix} = \begin{bmatrix} 1 & \xi & \eta & \xi\eta & \eta^2 & \xi\eta^2 & \eta^3 & \xi\eta^3 & 0 & 0 & 0 & 0 \\ 0 & 0 & 0 & 0 & 0 & 0 & 0 & 0 & 1 & \xi & \eta & \xi\eta \\ 0 & 0 & \dfrac{-2}{h} & \dfrac{-2\xi}{h} & \dfrac{-4\eta}{h} & \dfrac{-4\xi\eta}{h} & \dfrac{-6\eta^2}{h} & \dfrac{-6\xi\eta^2}{h} & 0 & 0 & 0 & 0 \end{bmatrix} \begin{pmatrix} \alpha_1 \\ \alpha_2 \\ \alpha_3 \\ \alpha_4 \\ \alpha_5 \\ \alpha_6 \\ \alpha_7 \\ \alpha_8 \\ \beta_1 \\ \beta_2 \\ \beta_3 \\ \beta_4 \end{pmatrix} \tag{1}$$

where

h = height of the panel zone.

Using the 12 boundary conditions at the four nodes of the element, the nodal degrees of freedom (u, v and θs) can be related to the generalized degrees of freedoms (α and βs) by

$$\begin{pmatrix} u_1 \\ u_2 \\ u_3 \\ u_4 \\ v_1 \\ v_2 \\ v_3 \\ v_4 \\ \theta_1 \\ \theta_2 \\ \theta_3 \\ \theta_4 \end{pmatrix} = \mathbf{C}_1\mathbf{C}_2 \begin{pmatrix} \alpha_1 \\ \alpha_2 \\ \alpha_3 \\ \alpha_4 \\ \alpha_5 \\ \alpha_6 \\ \alpha_7 \\ \alpha_8 \\ \beta_1 \\ \beta_2 \\ \beta_3 \\ \beta_4 \end{pmatrix} \tag{2}$$

where

$$\mathbf{C}_1 = \begin{bmatrix} 1 & & & & & & & & & & & \\ & 1 & & & & & & & & & & \\ & & 1 & & & & & & & & & \\ & & & 1 & & & & & & & & \\ & & & & 1 & & & & & & & \\ & & & & & 1 & & & & & & \\ & & & & & & 1 & & & & & \\ & & & & & & & 1 & & & & \\ & & & & & & & & \frac{-2}{h} & & & \\ & & & & & & & & & \frac{-2}{h} & & \\ & & & & & & & & & & \frac{-2}{h} & \\ & & & & & & & & & & & \frac{-2}{h} \end{bmatrix} \tag{3a}$$

$$\mathbf{C}_2 = \begin{bmatrix} 1 & -1 & -1 & 1 & 1 & -1 & -1 & 1 & 0 & 0 & 0 & 0 \\ 1 & -1 & 1 & -1 & 1 & -1 & 1 & -1 & 0 & 0 & 0 & 0 \\ 1 & 1 & 1 & 1 & 1 & 1 & 1 & 1 & 0 & 0 & 0 & 0 \\ 1 & 1 & -1 & -1 & 1 & 1 & -1 & -1 & 0 & 0 & 0 & 0 \\ 0 & 0 & 0 & 0 & 0 & 0 & 0 & 0 & 1 & -1 & -1 & 1 \\ 0 & 0 & 0 & 0 & 0 & 0 & 0 & 0 & 1 & -1 & 1 & -1 \\ 0 & 0 & 0 & 0 & 0 & 0 & 0 & 0 & 1 & 1 & 1 & 1 \\ 0 & 0 & 0 & 0 & 0 & 0 & 0 & 0 & 1 & 1 & -1 & -1 \\ 0 & 0 & 1 & -1 & -2 & 2 & 3 & -3 & 0 & 0 & 0 & 0 \\ 0 & 0 & 1 & -1 & 2 & -2 & 3 & -3 & 0 & 0 & 0 & 0 \\ 0 & 0 & 1 & 1 & 2 & 2 & 3 & 3 & 0 & 0 & 0 & 0 \\ 0 & 0 & 1 & 1 & -2 & -2 & 3 & 3 & 0 & 0 & 0 & 0 \end{bmatrix}. \tag{3b}$$

From eqn (2), we can write

$$\begin{pmatrix} \alpha_1 \\ \alpha_2 \\ \alpha_3 \\ \alpha_4 \\ \alpha_5 \\ \alpha_6 \\ \alpha_7 \\ \alpha_8 \\ \beta_1 \\ \beta_2 \\ \beta_3 \\ \beta_4 \end{pmatrix} = \mathbf{C}_2^{-1}\mathbf{C}_1^{-1} \begin{pmatrix} u_1 \\ u_2 \\ u_3 \\ u_4 \\ v_1 \\ v_2 \\ v_3 \\ v_4 \\ \theta_1 \\ \theta_2 \\ \theta_3 \\ \theta_4 \end{pmatrix}. \tag{4}$$

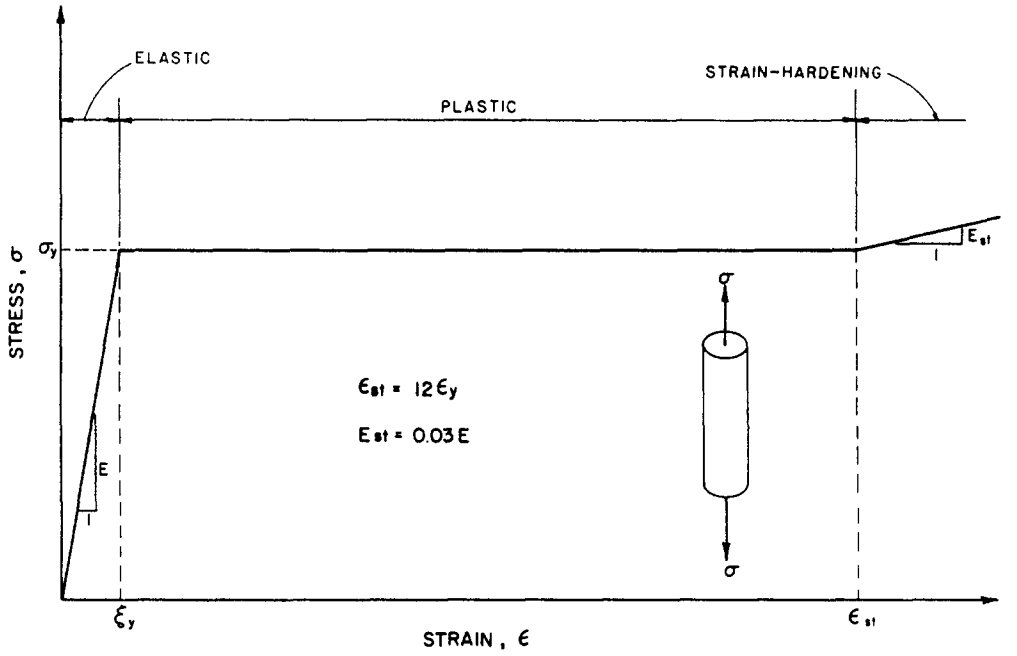

Fig. 5. Assumed uniaxial stress–strain behavior.

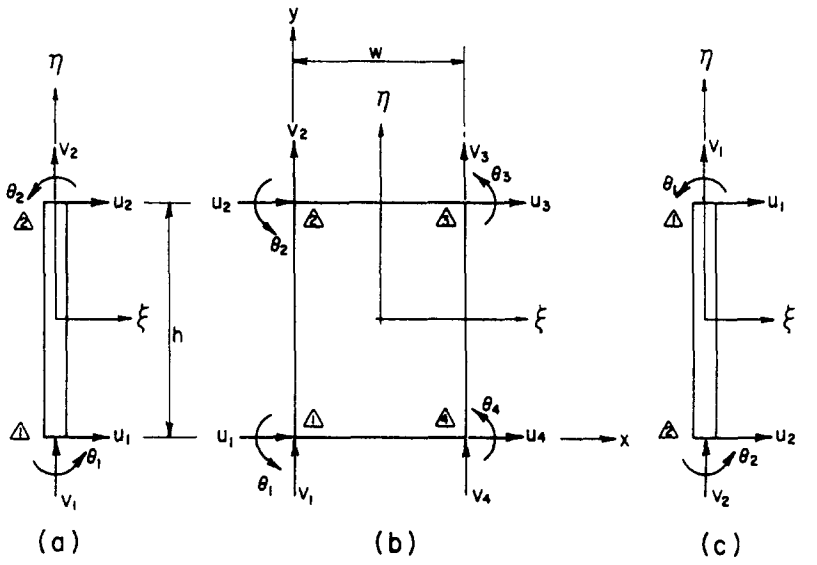

Fig. 6. Finite element model of the web and flanges of a joint panel.

Upon substitution of eqn (4) into eqn (1) and rearrangement gives

$$\begin{pmatrix} u \\ v \\ \theta \end{pmatrix} = \begin{bmatrix} N_{u1} & 0 & N_{u2} & N_{u3} & 0 & N_{u4} & N_{u5} & 0 & N_{u6} & N_{u7} & 0 & N_{u8} \\ 0 & N_{v1} & 0 & 0 & N_{v2} & 0 & 0 & N_{v3} & 0 & 0 & N_{v4} & 0 \\ N_{\theta 1} & 0 & N_{\theta 2} & N_{\theta 3} & 0 & N_{\theta 4} & N_{\theta 5} & 0 & N_{\theta 6} & N_{\theta 7} & 0 & N_{\theta 8} \end{bmatrix} \begin{pmatrix} u_1 \\ v_1 \\ \theta_1 \\ u_2 \\ v_2 \\ \theta_2 \\ u_3 \\ v_3 \\ \theta_3 \\ u_4 \\ v_4 \\ \theta_4 \end{pmatrix} \tag{5}$$

where

$$N_{u1} = \tfrac{1}{8}(2-3\eta+\eta^3)(1-\xi)$$

$$N_{u2} = \frac{-h}{16}(1-\eta-\eta^2+\eta^3)(1-\xi)$$

$$N_{u3} = \tfrac{1}{8}(2+3\eta-\eta^3)(1-\xi)$$

$$N_{u4} = \frac{-h}{16}(-1-\eta+\eta^2+\eta^3)(1-\xi)$$

$$N_{u5} = \tfrac{1}{8}(2+3\eta-\eta^3)(1+\xi)$$

$$N_{u6} = \frac{-h}{16}(-1-\eta+\eta^2+\eta^3)(1+\xi)$$

$$N_{u7} = \tfrac{1}{8}(2-3\eta+\eta^3)(1+\xi)$$

$$N_{u8} = \frac{-h}{16}(1-\eta-\eta^2+\eta^3)(1+\xi)$$

$$N_{v1} = \tfrac{1}{4}(1-\xi)(1-\eta)$$

$$N_{v2} = \tfrac{1}{4}(1-\xi)(1+\eta)$$

$$N_{v3} = \tfrac{1}{4}(1+\xi)(1+\eta)$$

$$N_{v4} = \tfrac{1}{4}(1+\xi)(1-\eta)$$

$$N_{\theta 1} = \frac{-1}{4h}(1-\xi)(-3+3\eta^2)$$

$$N_{\theta 2} = \tfrac{1}{8}(1-\xi)(-1-2\eta+3\eta^2)$$

$$N_{\theta 3} = \frac{-1}{4h}(1-\xi)(3-3\eta^2)$$

$$N_{\theta 4} = \tfrac{1}{8}(1-\xi)(-1+2\eta+3\eta^2)$$

$$N_{\theta 5} = \frac{-1}{4h}(1+\xi)(3-3\eta^2)$$

$$N_{\theta 6} = \tfrac{1}{8}(1+\xi)(-1+2\eta+3\eta^2)$$

$$N_{\theta 7} = \frac{-1}{4h}(1+\xi)(-3+3\eta^2)$$

$$N_{\theta 8} = \tfrac{1}{8}(1+\xi)(-1-2\eta+3\eta^2).$$

Symbolically, eqn (5) can be written as

$$\mathbf{u}_w = \mathbf{N}_w \mathbf{d}_w \tag{6}$$

The next step in evaluating the element stiffness matrix using the finite element method is to formulate the strain–displacement relationship. The strain–displacement relationship can be written as

$$\boldsymbol{\varepsilon}_w = \begin{pmatrix} \varepsilon_x \\ \varepsilon_y \\ \gamma_{xy} \end{pmatrix} = \begin{bmatrix} 1000 \\ 0001 \\ 0110 \end{bmatrix} \begin{bmatrix} \mathbf{J}^{-1} & \\ & \mathbf{J}^{-1} \end{bmatrix} \begin{bmatrix} \frac{\partial}{\partial \xi} & 0 & 0 \\ \frac{\partial}{\partial \eta} & 0 & 0 \\ 0 & \frac{\partial}{\partial \xi} & 0 \\ 0 & \frac{\partial}{\partial \eta} & 0 \end{bmatrix} \mathbf{N}_w \mathbf{d}_w. \tag{7}$$

where $\mathbf{J}^{-1}$ is the inverse of the Jacobian matrix given by

$$\mathbf{J}^{-1} = \begin{bmatrix} \frac{\partial x}{\partial \xi} & \frac{\partial y}{\partial \xi} \\ \frac{\partial x}{\partial \eta} & \frac{\partial y}{\partial \eta} \end{bmatrix}^{-1} = \begin{bmatrix} \frac{w}{2} & 0 \\ 0 & \frac{h}{2} \end{bmatrix}^{-1} = \begin{bmatrix} \frac{2}{w} & 0 \\ 0 & \frac{2}{h} \end{bmatrix}. \tag{8}$$

Carrying out the matrix manipulation, eqn (7) can be written as

$$\boldsymbol{\varepsilon}_w = \mathbf{B}_w \mathbf{d}_w \tag{9}$$

where

$$\mathbf{B}_w = \begin{bmatrix} \frac{-1}{4w}(2-3\eta+\eta^3) & 0 & \frac{h}{8w}(1-\eta-\eta^2+\eta^3) \\ 0 & \frac{-1}{2h}(1-\xi) & 0 \\ \frac{1}{4h}(1-\xi)(-3+3\eta^2) & \frac{-1}{2w}(1-\eta) & \frac{1}{8}(1-\xi)(-1-2\eta+3\eta^2) \end{bmatrix}$$

$$\begin{bmatrix} \frac{-1}{4w}(2+3\eta-\eta^3) & 0 & \frac{h}{8w}(-1-\eta+\eta^2+\eta^3) \\ 0 & \frac{1}{2h}(1-\xi) & 0 \\ \frac{1}{4h}(1-\xi)(3-3\eta^2) & \frac{-1}{2w}(1+\eta) & \frac{-1}{8}(1-\xi)(-1+2\eta+3\eta^2) \end{bmatrix}$$

$$\begin{bmatrix} \frac{1}{4w}(2+3\eta-\eta^3) & 0 & \frac{-h}{8w}(-1-\eta+\eta^2+\eta^3) \\ 0 & \frac{1}{2h}(1+\xi) & 0 \\ \frac{1}{4h}(1+\xi)(3-3\eta^2) & \frac{1}{2w}(1+\eta) & \frac{-1}{8}(1+\xi)(-1+2\eta+3\eta^2) \end{bmatrix}$$

$$\begin{bmatrix} \frac{1}{4w}(2-3\eta+\eta^3) & 0 & \frac{-h}{8w}(1-\eta-\eta^2+\eta^3) \\ 0 & \frac{-1}{2h}(1+\xi) & 0 \\ \frac{1}{4h}(1+\xi)(-3+3\eta^2) & \frac{1}{2w}(1-\eta) & \frac{-1}{8}(1+\xi)(-1-2\eta+3\eta^2) \end{bmatrix} \tag{10}$$

in which

h = height of the panel zone
W = width of the panel web.

Having developed the strain–displacement relationship, the stiffness matrix of the web of the panel zone can be written as

$$\mathbf{k}_w = \int_V \mathbf{B}_w^T \mathbf{D} \mathbf{B}_w \, dV = t_w \int_{-1}^{1} \int_{-1}^{1} \mathbf{B}_w^T \mathbf{D} \mathbf{B}_w |J| \, d\xi \, d\eta \tag{11}$$

where

t_w = thickness of the column web in the panel zone

$$|J| = \begin{vmatrix} \frac{w}{2} & \cdot \\ \cdot & \frac{h}{2} \end{vmatrix} = \frac{hw}{4}$$

$$\mathbf{D} = \begin{cases} \mathbf{D}^e & \text{if the panel web element is elastic} \\ \mathbf{D}^{ep} & \text{if the panel web element has yielded} \end{cases}$$

in which

$$\mathbf{D}^e = \frac{E}{1-\nu^2} \begin{bmatrix} 1 & \nu & 0 \\ \nu & 1 & 0 \\ 0 & 0 & \frac{1-\nu}{2} \end{bmatrix}$$

$\mathbf{D}^{ep}$ = elastic–plastic stress–strain relationship (eqn 32).

Equation (11) can be integrated numerically by using a 2×4 Gauss–Legendre Quadrature (Fig. 7), i.e.

$$k_w = \frac{hwt_w}{4} \sum_{i=1}^{2} \sum_{j=1}^{4} W_i W_j [\mathbf{B}_w^T \mathbf{D} \mathbf{B}_w]_{\xi=\xi_i, \eta=\eta_j} \tag{12}$$

where W_i, W_j are weight coefficients (Table 1).

$\mathbf{k}_w$ expressed in eqn (12) is the stiffness matrix of the web element of the panel zone with reference to a local coordinate system. The incremental form of this stiffness matrix is the same as $\mathbf{k}_w$ since the entries of $\mathbf{k}_w$ are independent of the displacement, i.e.

$$\dot{\mathbf{k}}_w = \mathbf{k}_w. \tag{13}$$

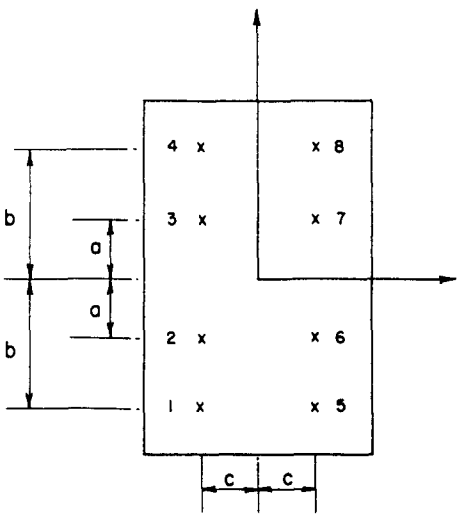

Fig. 7. Gauss points of the panel web element.

Flange element

The local (ξ, η) coordinate system and the degrees of freedom of the two flange elements for the panel zone are shown in Figs 6(a) and (c), respectively.

For simplicity, the stiffness matrices used for these flange elements are those of the ordinary frame element, i.e.

for the left flange:

$$\mathbf{k}_{lj} = \frac{EI_f}{h^3}\begin{bmatrix} 12 & 0 & -6h & -12 & 0 & -6h \\ & \frac{h^2A_f}{I} & 0 & 0 & \frac{-h^2A_f}{I} & 0 \\ & & 4h^2 & 6h & 0 & 2h^2 \\ & & & 12 & 0 & 6h \\ & \text{sym.} & & & \frac{h^2A_f}{I} & 0 \\ & & & & & 4h^2 \end{bmatrix} \tag{14}$$

and for the right flange:

$$\mathbf{k}_{rf} = \frac{EI_f}{h^3}\begin{bmatrix} 12 & 0 & 6h & -12 & 0 & 6h \\ & \frac{h^2A_f}{I} & 0 & 0 & \frac{-h^2A_f}{I} & 0 \\ & & 4h^2 & -6h & 0 & 2h^2 \\ & & & 12 & 0 & -6h \\ & \text{sym.} & & & \frac{h^2A_f}{I} & 0 \\ & & & & & 4h^2 \end{bmatrix}; \tag{15}$$

Table 1. Weight coefficients

Gauss point	W_i	W_j
1	1.00000	0.34785
2	1.00000	0.65215
3	1.00000	0.65215
4	1.00000	0.34785
5	1.00000	0.34785
6	1.00000	0.65215
7	1.00000	0.65215
8	1.00000	0.34785

where

h = height of panel zone

$$I_f = \frac{1}{12} b_f t_f^3$$

$$A_f = b_f t_f$$

in which

b_f = width of column flange

t_f = thickness of column flange.

The corresponding incremental forms of $\mathbf{k}_{1f}$ and $\mathbf{k}_{rf}$ are

$$\dot{\mathbf{k}}_{1f} = \mathbf{k}_{1f} \tag{16}$$

and

$$\dot{\mathbf{k}}_{rf} = \mathbf{k}_{rf} \tag{17}$$

respectively.

With the incremental stiffness matrices for the three elements of the panel zone (Figs 6(a)–(c)) developed, the incremental stiffness matrix $\dot{\mathbf{k}}_{1p}$ of the panel zone (Fig. 8)

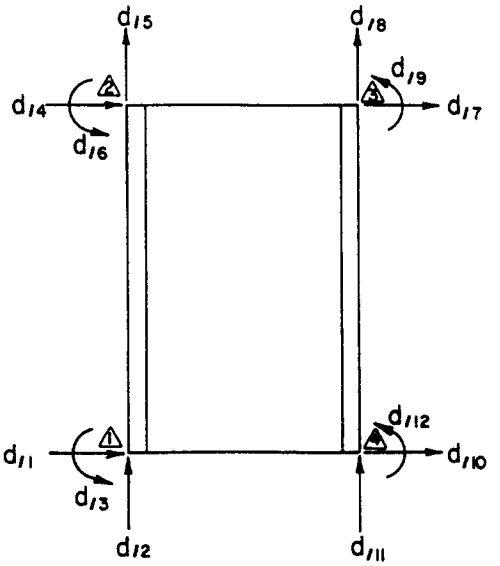

Fig. 8. Degrees of freedom of a joint panel in local coordinate.

with respect to a local coordinate system can be obtained by assemblage

$$\dot{\mathbf{k}}_{1p} = \text{assembling } \mathbf{T}_{olf}^T \dot{\mathbf{k}}_{lf} \mathbf{T}_{olf} \quad \mathbf{T}_{ow}^T \dot{\mathbf{k}}_w \mathbf{T}_{ow} \quad \mathbf{T}_{orf}^T \dot{\mathbf{k}}_{rf} \mathbf{T}_{orf}; \tag{18}$$

where

$$\mathbf{T}_{olf} = \text{offset transformation matrix of the left flange element} = \begin{bmatrix} \mathbf{H}_{lf} & 0 \\ 0 & H_{lf} \end{bmatrix} \tag{19}$$

in which

$$\mathbf{H}_{lf} = \begin{bmatrix} 1 & 0 & 0 \\ 0 & 1 & \frac{t_f}{2} \\ 0 & 0 & 1 \end{bmatrix}. \tag{20}$$

$$\mathbf{T}_{ow} = \text{offset transformation matrix of the web element} = \begin{bmatrix} \mathbf{H}_{lw} & \cdot & \cdot & \cdot \\ \cdot & H_{lw} & \cdot & \cdot \\ \cdot & \cdot & H_{rw} & \cdot \\ \cdot & \cdot & \cdot & H_{rw} \end{bmatrix}, \tag{21}$$

in which

$$\mathbf{H}_{lw} = \begin{bmatrix} 1 & 0 & 0 \\ 0 & 1 & t_f \\ 0 & 0 & 1 \end{bmatrix} \tag{22}$$

$$\mathbf{H}_{rw} = \begin{bmatrix} 1 & 0 & 0 \\ 0 & 1 & -t_f \\ 0 & 0 & 1 \end{bmatrix}. \tag{23}$$

$$\mathbf{T}_{orf} = \text{offset transformation matrix of the right flange element} = \begin{bmatrix} \mathbf{H}_{rf} & \cdot \\ \cdot & \mathbf{H}_{rf} \end{bmatrix} \tag{24}$$

in which

$$\mathbf{H}_{rf} = \begin{bmatrix} 1 & 0 & 0 \\ 0 & 1 & \frac{-t_f}{2} \\ 0 & 0 & 1 \end{bmatrix}. \tag{25}$$

In the above equations, t_f is the thickness of the column flange.

These offset transformation matrices are needed due to the fact that the degrees of freedom of the web and flange elements (Figs 6(a)–(c)) do not coincide with that of the

panel element (Fig. 8). In writing these matrices, it is tacitly assumed that the through-thickness and shear strains of the flanges of the column are negligible. These assumptions are conformable with experimental observations.

The incremental stiffness matrix expressed in eqn (18) was developed with respect to a local coordinate system which translates and rotates with the element. To incorporate the panel element in a general frame analysis, this stiffness matrix must be expressed with respect to a fixed or global coordinate system. The incremental stiffness matrix of the panel element expressed with respect to a fixed (X, Y) coordinate system is given by

$$\dot{\mathbf{k}}_{gp} = \mathbf{T}_{lg}^{T}\dot{\mathbf{k}}_{lp}\mathbf{T}_{lg} \tag{26}$$

where

$$\mathbf{T}_{lg} = \begin{bmatrix} \mathbf{t}_{lg} & \cdot & \cdot & \cdot \\ \cdot & t_{lg} & \cdot & \cdot \\ \cdot & \cdot & t_{lg} & \cdot \\ \cdot & \cdot & \cdot & t_{lg} \end{bmatrix} \tag{27}$$

in which

$$\mathbf{t}_{lg} = \begin{bmatrix} \cos\theta_{lg} & \sin\theta_{lg} & 0 \\ -\sin\theta_{lg} & \cos\theta_{lg} & 0 \\ 0 & 0 & 1 \end{bmatrix} \tag{28}$$

where (see Fig. 9)

$$\theta_{lg} = \frac{1}{4}\left(\tan^{-1}\frac{d_{g1}-d_{g4}}{h+d_{g5}-d_{g2}} + \tan^{-1}\frac{d_{g8}-d_{g5}}{w+d_{g7}-d_{g4}} + \tan^{-1}\frac{d_{g10}-d_{g7}}{h+d_{g8}-d_{g11}} + \tan^{-1}\frac{d_{g11}-d_{g2}}{w+d_{g10}-d_{g1}}\right). \tag{29}$$

Panel zone plasticity

When the state of stress of the panel web reaches a limit defined by the Von Mises (or J_2) theory

$$f = J_2 - \frac{\sigma_y^2}{3} = 0 \tag{30}$$

where, for plane stress case

$J_2 = \frac{1}{3}(\sigma_{xx}^2 - \sigma_{xx}\sigma_{yy} + \sigma_{yy}^2 + 3\tau_{xy}^2)$

σ_y = yield stress of the material a uniaxial tension test (Fig. 5)

the column web of the panel zone is assumed to be yielded.

If strain-hardening of the material is considered (Fig. 5), then in addition to describing the initial yield surface (eqn (30)), we need to define a subsequent yield (or loading) surface. If isotropic hardening is assumed in which the loading surface is described by a uniform expansion of the initial yield surface, then eqn (30) can be generalized to

$$f = J_2 - k^2 = 0 \tag{31}$$

where k is the hardening parameter.

Once eqn (30) or eqn (31) is satisfied, the elastic–plastic stress–strain matrix $\mathbf{D}^{ep}$ will be used in place of the elastic stress–strain matrix $\mathbf{D}^{e}$ in evaluating $\mathbf{k}_w$ in eqn (11) or (12).

The elastic–plastic stress–strain matrix is given (3) by

$$\mathbf{D}^{ep} = \mathbf{D}^{e} - \frac{\mathbf{D}^{e}\left(\frac{\partial f}{\partial \sigma}\right)\left(\frac{\partial f}{\partial \sigma}\right)^{T}\mathbf{D}^{e}}{\left(\frac{\partial f}{\partial \sigma}\right)^{T}\mathbf{D}^{e}\left(\frac{\partial f}{\partial \sigma}\right)+A} \tag{32}$$

where, for J_2 theory and associate flow rule, for plane stress case,

$$\mathbf{D}^{e} = \text{elastic stress–strain matrix}$$

$$\frac{\partial f}{\partial \sigma} = \mathbf{S} = \text{deviatoric stress vector}$$

$$= \begin{bmatrix} \dfrac{2\sigma_{xx}-\sigma_{yy}}{2} \\ \dfrac{2\sigma_{yy}-\sigma_{xx}}{3} \\ 2\tau_{xy} \end{bmatrix} \tag{33}$$

$$A = \frac{4\sqrt{3}}{9}\sigma_e^2 H' \tag{34}$$

in which

$$\sigma_e = \sqrt{(\sigma_{xx}^2 - \sigma_{xx}\sigma_{yy} + \sigma_{yy}^2 + 3\tau_{xy}^2)} \tag{35}$$

$$H' = \frac{dk}{d\varepsilon_p} = \begin{cases} 0 & \text{if } \varepsilon_p \leqslant 11\varepsilon_y \\ \dfrac{1}{\sqrt{3}}\dfrac{EE_{st}}{E-E_{st}} & \text{if } \varepsilon_p > 11\varepsilon_y \end{cases} \tag{36}$$

H' is the slope of the hardening parameter k vs the effective strain ε_p plot (Fig. 10). Note that $\mathbf{D}^{ep}$ is a function of the state of stress and the effective strain.

In the numerical analysis, once eqn (30) or (31) is satisfied, this elastic–plastic stress–strain matrix is used in place of the elastic stress–strain matrix in evaluating the panel incremental stiffness matrix. It should be noted that in many instances, the yield condition will be violated. A finite load increment may bring the state of stress of the element outside the yield surface (point Q in Fig. 11). If this is the case, the load increment is scaled down by a factor r defined as

$$r = \frac{-b+\sqrt{b^2-4ac}}{2a} \tag{37}$$

where

$$a = \dot{\sigma}_{xx}^2 + \dot{\sigma}_{yy}^2 - \dot{\sigma}_{xx}\dot{\sigma}_{yy} + 3\dot{\tau}_{xy}^2$$

$$b = 2\sigma_{xx}\dot{\sigma}_{xx} + 2\sigma_{yy}\dot{\sigma}_{yy} - \sigma_{xx}\dot{\sigma}_{yy} - \sigma_{yy}\dot{\sigma}_{xx} + 6\tau_{xy}\dot{\tau}_{xy}$$

$$c = \sigma_{xx}^2 + \sigma_{yy}^2 - \sigma_{xx}\sigma_{yy} + 3\tau_{xy}^2 - 3k^2$$

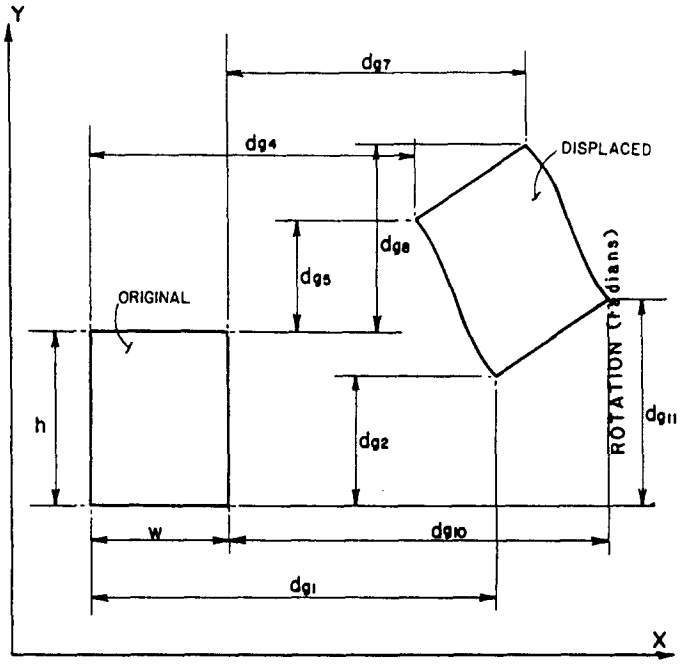

Fig. 9. Global displacements of the panel element.

in which

$\dot{\sigma}_{ij}$ = increment of stress induced by the load increment (Fig. 11) assuming elastic behavior
σ_{ij} = state of stress before the load increment (point P in Fig. 11)
k = hardening parameter (Fig. 10).

This scaling procedure is repeated until eqn (30) or (31) is satisfied, i.e. until the state of stress of the element is at point R in Fig. 11.

In order to check the yield criterion of eqn (30) or (31), the current state of stress of the element must be known. Since the strains and hence the stresses vary from point to point in the element, sample points must be chosen in such a way as to represent the state

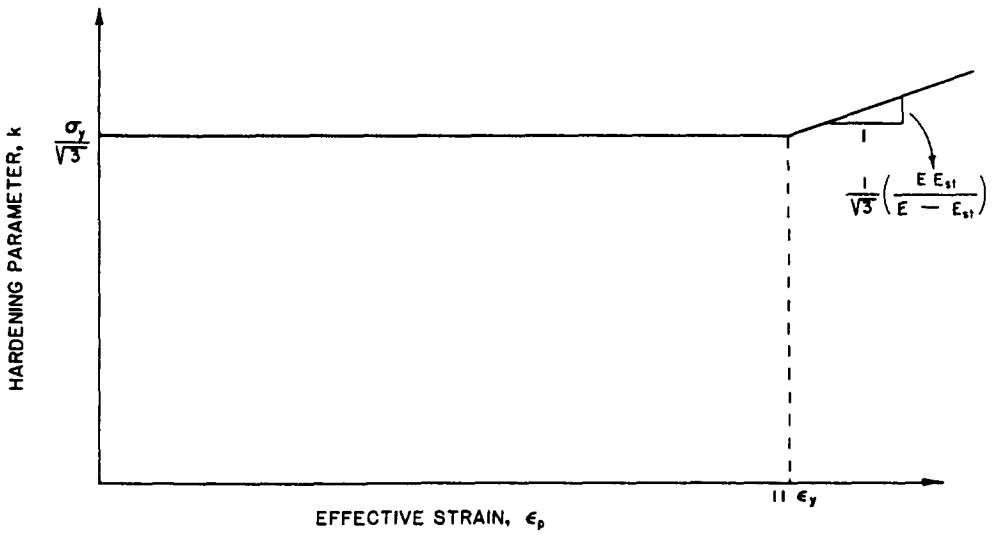

Fig. 10. $k-\varepsilon_p$ plot.

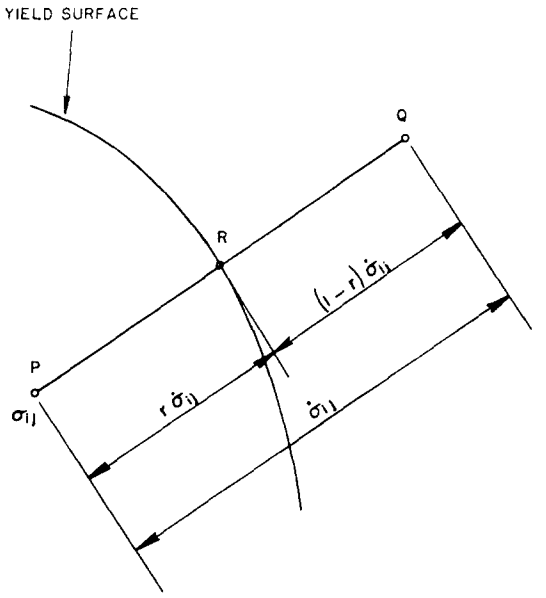

Fig. 11. Scaling back to yield surface.

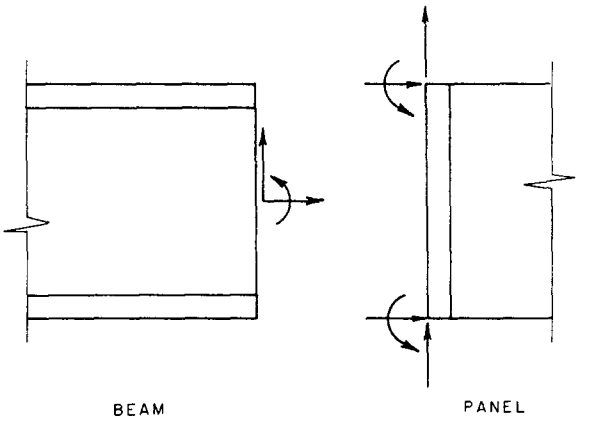

Fig. 12. Junction of a beam–column and a panel element.

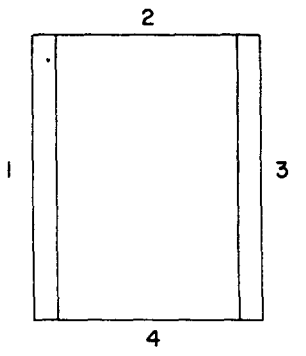

Fig. 13. Face numbering of a panel element.

of the element in the best possible way in the numerical analysis. In the present study, the eight Gauss points (Fig. 7) and the centroid of the element are used as the sample points. Detailed calculations of stresses at these points are discussed in [8].

MODIFICATION OF INCREMENTAL BEAM–COLUMN STIFFNESS MATRIX FOR THE PRESENCE OF PANEL ZONE

If a panel element is present at the end of a frame element, the 3 degrees of freedom at the end of the frame element must be related to the 6 degrees of freedom on the face of the panel element (Fig. 12). In order to relate the degrees of freedom of these two elements, the concept of equivalent nodal force used in the context of a finite element analysis is utilized. The forces (axial, shear, moment) at the end of the frame element are regarded as the applied forces and the energy equivalent forces developed at the nodes of the panel element are evaluated using the energy balanced concept. The resulting matrix relating the two sets of forces is the equilibrium matrix. Transposition of this matrix will give the kinematic matrix which relates the degrees of freedom of the two elements.

Depending on the face of the panel element (Fig. 13) to which the frame element is attached and the manner the frame forces are assumed to be distributed (Fig. 14) on the panel face, several different cases can be identified. It should be mentioned that faces 1 and 3 should be treated differently than faces 2 and 4. This is because a frame element attaches to face 1 or 3 of the panel element through a connection. Whereas, for face 2 or 4, the junction of the frame and panel elements are physically continuous. In this context, a connection element[8] was inserted between the frame and panel elements for faces 1 and 3 and a stiffener element[8] with high bending rigidity was inserted between the frame and panel elements for faces 2 and 4. The assumed force distribution shown in Fig. 14 is for faces 1 and 3 only. Category A is appropriate for such types of connections in which continuity between the two elements exists along the depth or at the two flanges of the frame element (Fig. 15(a)). Examples for this category of connections are top and seat angles, header plate, end plate and T-stub connections. Category B is appropriate for such

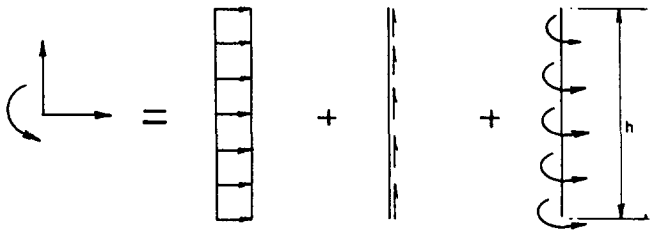

(a) CATEGORY A

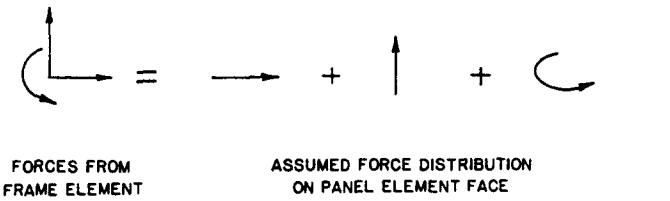

(b) CATEGORY B

Fig. 14. Assumed force distributions on faces 1 and 3 of the panel element.

connections in which continuity exists more or less at the neutral axis of the frame element (Fig. 15(b)). Examples for this category of connections are single web angle and double web angle connections. The kinematic matrices relating the degrees of freedom of the two elements (frame and panel) for different faces of the panel element and different categories of connections were developed in detail in [8] and are summarized in Appendix I.

Once the kinematic matrices are known, the 6×6 frame element can be modified to a 9×9 frame element with a panel attached to one of its ends as follows.

If a panel is present at the Ath end of the frame element

$$\dot{\mathbf{k}}_{fm} = \begin{bmatrix} \mathbf{T}_{fp}^T & \cdot \\ \cdot & \mathbf{I}^T \end{bmatrix} \dot{\mathbf{k}}_f \begin{bmatrix} \mathbf{T}_{fp} & \cdot \\ \cdot & \mathbf{I} \end{bmatrix}. \tag{38}$$

If a panel is present at the Bth end of the frame element

$$\dot{\mathbf{k}}_{fm} = \begin{bmatrix} \mathbf{I}^T & \cdot \\ \cdot & \mathbf{T}_{fp}^T \end{bmatrix} \dot{\mathbf{k}}_f \begin{bmatrix} \mathbf{I} & \cdot \\ \cdot & \mathbf{T}_{fp} \end{bmatrix} \tag{39}$$

where, in eqns (38) and (39)

$\dot{\mathbf{k}}_{fm}$ $= 9 \times 9$ modified frame element tangent stiffness matrix
$\mathbf{k}_f$ $= 6 \times 6$ frame element tangent stiffness matrix (see Appendix II)
$\mathbf{T}_{fp}$ $= 3 \times 6$ kinematic matrix relating the 3 degrees of freedom at the end of the frame element to the 6 degrees of freedom on the face of the panel element
$\mathbf{I}$ $= 3 \times 3$ identity matrix.

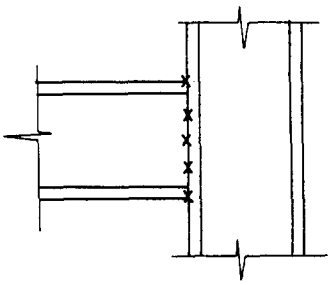

(a) CATEGORY A

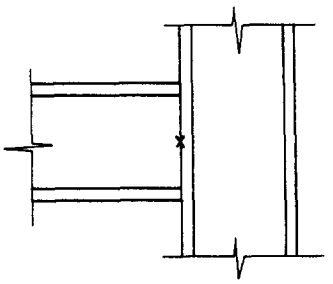

(b) CATEGORY B

x REGION OF ATTACHMENT OF A FRAME ELEMENT TO A PANEL

Fig. 15. Category A and category B connections.

Note that the modified incremental stiffness matrix of the frame element is 9×9 which means 3 additional degrees of freedom are introduced into the frame element (see Fig. 16).

If a plastic hinge or connection exists at the end of the frame element, modifications to $\dot{\mathbf{k}}_f$ are first performed[8] and then used in place of the original $\dot{\mathbf{k}}_f$.

NUMERICAL STUDIES

The panel element developed here is used in conjunction with the frame and connection elements developed in a separate report[8] to investigate the behavior of frames. A load-controlled incremental Newton–Raphson iterative solution technique is employed in the numerical analysis. Detailed discussion of the solution algorithm is given elsewhere[8]. In this section, the validity of the panel zone model is first verified by comparison of the numerical results with experiments. A simple two-bar frame is then analyzed using different behavioral models regarding the deformational behavior of the connection and panel zone to demonstrate the effect of joint flexibility on the behavior of the frame.

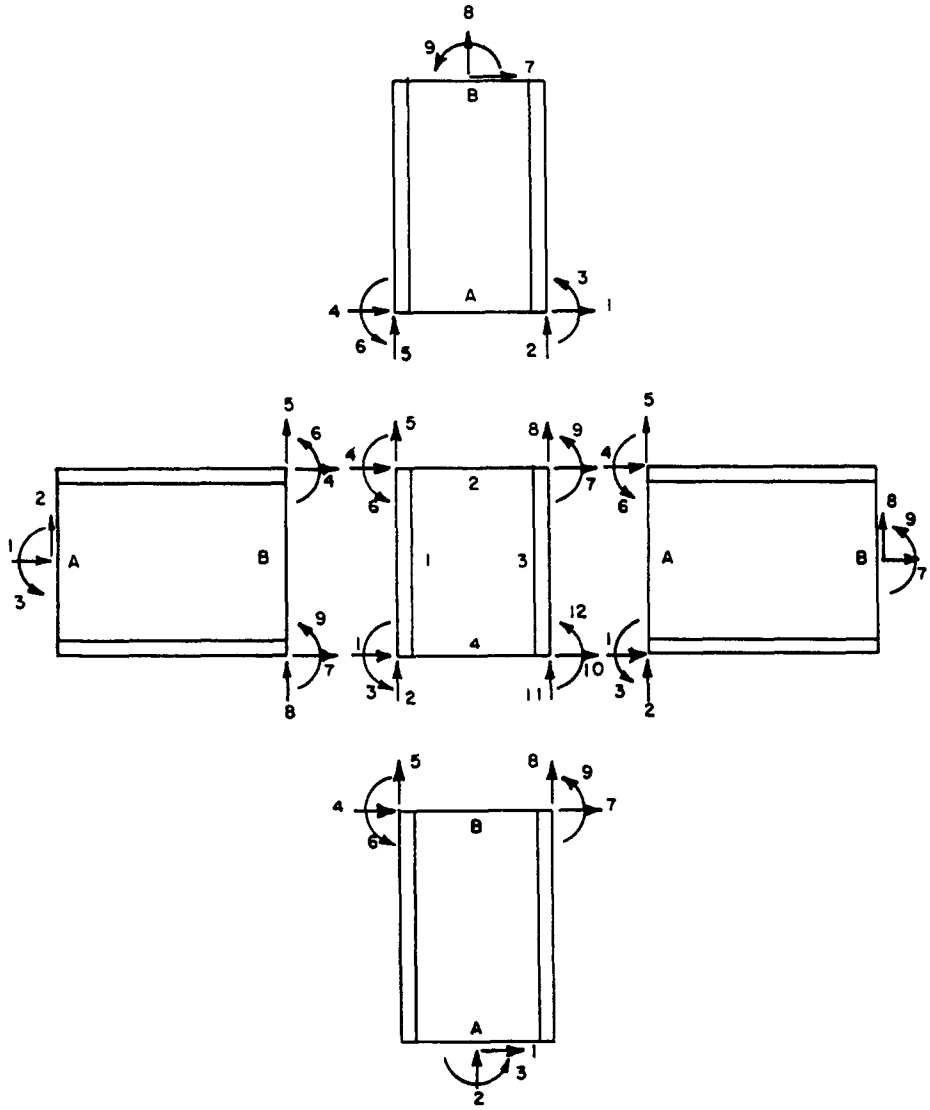

Fig. 16. Sign convention for the modified frame element.

COMPARISON WITH EXPERIMENTS

Shown in the inset of Fig. 17 is a subassemblage used by Fielding and Huang[4] to investigate the behavior of the joint panel. The joint details of the subassemblage are given in [4]. The column was first loaded with a compressive force of 0.5 P_y where P_y is the yield load of the column. The beam load was then applied at the free end of the beam until failure. During the entire beam loading phase, the column load was maintained at 0.5 P_y. As a result, the panel zone is under a combined loading of axial force from the column load and shear and moment from the beam load. The experimental load–deflection behavior of this subassemblage is shown in Fig. 17. Yielding of the web of the panel zone occurs at a load of 86 kips (383 kN) after which a definite decrease in stiffness of the joint panel was observed. At 150 kips (667 kN), cracks were observed at the ends of the top horizontal stiffeners and the specimen was unloaded. Also shown in this figure as a dashed line, is the numerically obtained load–deflection curve. It can be seen that good correlation exists between the results obtained numerically and experimentally both in the elastic and post-yield regimes. In the numerical solution, the actual measured[4] material properties were used. The apparent larger stiffness and higher yield load obtained numerically as compared to the test is attributed to the assumption of full fixity at both ends of the column in the numerical model, whereas in reality, noticeable column end rotations were observed[4].

The insets of Figs 18 and 19 show two subassemblages (Specimens A and B) of an experimental investigation of the behavior of panel zone by Bertero *et al.*[2]. Specimen A is typical of an upper story and Specimen B is typical of a lower story. For Specimen A, an axial force of 0.36 P_y, where P_y is the yield load of the column, was applied to the column

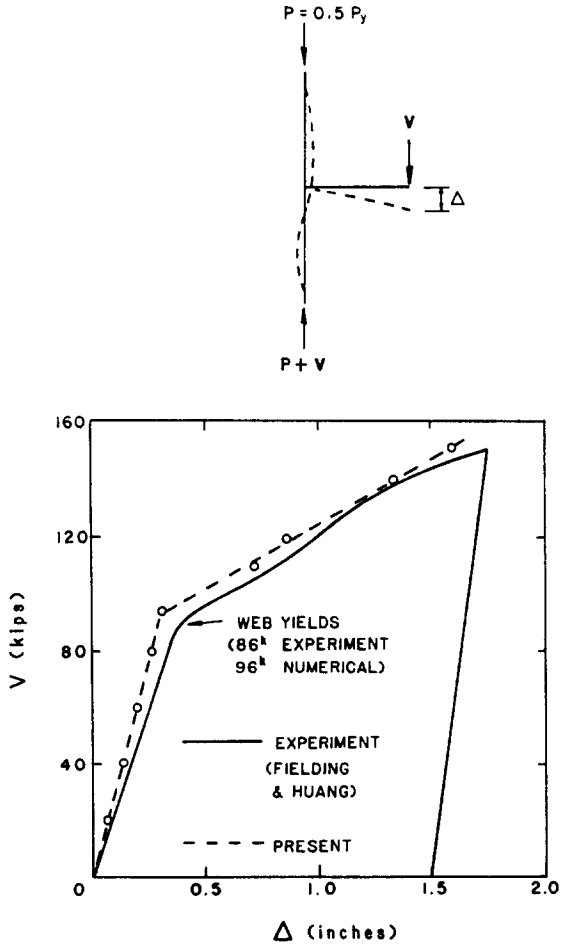

Fig. 17. Comparison of numerical and experimental connection subassemblage load–deflection behavior[4] (1 kip = 4.45 kN, 1 in. = 25.4 mm).

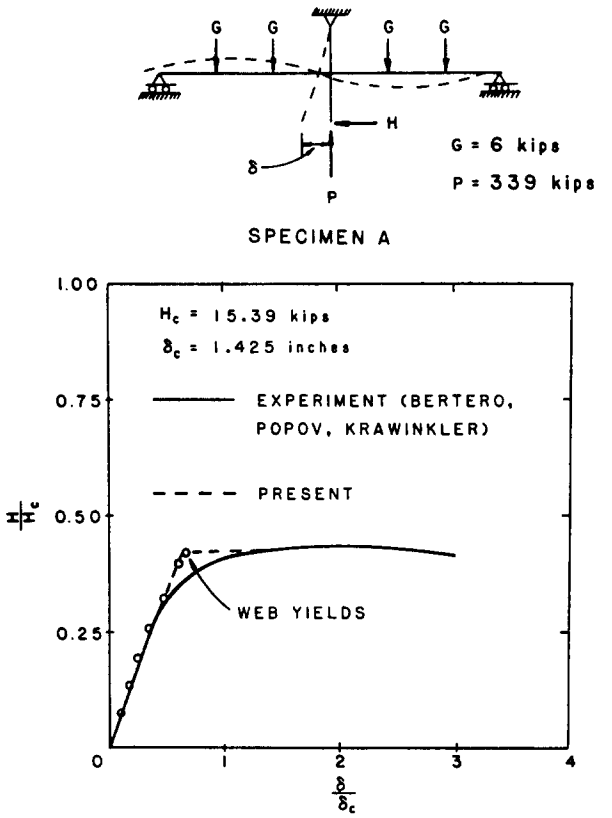

Fig. 18. Comparison of numerical and experimental connection subassemblage load–deflection behavior (Specimen B[2]) (1 kip = 4.45 kN, 1 in. = 25.4 mm).

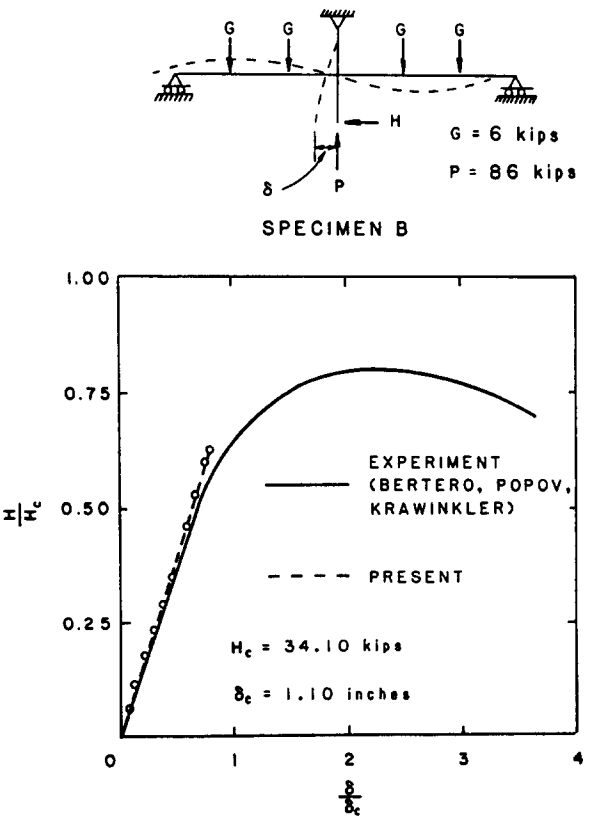

Fig. 19. Comparison of numerical and experimental connection subassemblage load–deflection behavior (Specimen B[2]) (1 kip = 4.45 kN, 1 in. = 25.4 mm).

and vertical beam forces of approx. 6 kips (27 kN) were applied at every third point on the beams. For Specimen B, an axial force of 0.48 P_y was applied to the column and vertical beam forces of approx. 6 kips (27 kN) were applied at every third point on the beams. These subassemblages were then subjected to a horizontal force H applied cyclically at the free end of the column. Since the present analysis deals only with monotonic loadings, only the initial branch of the hysteresis load–deflection behavior of these subassemblages will be investigated. The experimental curves are shown as solid lines in Figs 18 and 19 for Specimen A and B, respectively. For Specimen A (Fig. 18), extensive yielding of the web of the joint panel was observed in the test. The numerically obtained load–deflection curve using the actual measured[2] material properties is shown as a dashed line in the figure. Good agreement between the two curves is observed. The numerically predicted yielding of the web occurs at $H = 6.4$ kips (28 kN) which agrees favorably with the experiment. Since no stiffeners are used in the panel zone, the structure becomes numerically unstable as soon as the panel yields (that is, as soon as a panel hinge is formed). Consequently, the numerically generated load–deflection curve shows a plateau at $H = 6.4$ kips (28 kN).

The numerical and experimental load–deflection curves for Specimen B (Fig. 19) also agree well with each other. Failure of this specimen was due to the formation of plastic hinges in the beams. In the numerical solution, convergence of solution became impossible when a local collapse mechanism developed in the left beam at $H = 21.2$ kips (94.3 kN). However, in the experiment, additional load can be applied because even after the formation of a local collapse mechanism in the left beam, the subassemblage is still statically determinate and so total collapse will not occur until a third hinge forms in the right beam. Consequently, the experimental load–deflection curve rises above $H = 6.4$ kips (28 kN).

Although the post-yield behavior of the specimen shown in Fig. 19 cannot be predicted by the model due to local failure of the beam, the model does give a good representation of the elastic behavior of the subassemblage.

In the practical design, it is customary to investigate the drift (that is, lateral displacement) of a frame under service loading conditions to ensure that the frame will not deflect excessively so as to cause discomfort to the occupants of overstress in the connecting elements. In the following section, a simple two-bar frame will be analyzed using a number of different behavioral models to demonstrate the importance of panel zone deformation on the drift of a structure.

Analysis of a two-bar frame

Shown in Fig. 20 is a series of structural models for a two-bar frame. Model 1 (M1) is the conventional structural model commonly used by engineers and designers. The connection joining the beam and column is assumed to be rigid and center-to-center distances are used for the lengths of the beam and column. Model 2 (M2) is a more refined model. Although center-to-center distances are still used for the lengths of the beam and column, the connection is modeled by a spring having a rotational stiffness as described by the nonlinear moment–rotation behavior of the connection. Model 3 (M3) assumes that the connection is rigid but the finite size and deformable capability of the panel zone are taken into account. In this model, clear spans are used for the lengths of the beam and column. Model 4 (M4) is the most refined model of all. The connection is modeled as flexible with rotational stiffness described by the nonlinear moment–rotational behavior of the connection and the joint panel is modeled as deformable with clear spans used for the lengths of the beam and column.

For Models 2 and 4, the moment–rotation characteristics of four commonly used connections (double web angles, top and seat angles, end plate and T-stub) compatible with the beam and column sections (W14 × 34) used are shown in Fig. 21. They are labeled as C1, C2, C3 and C4, respectively. C1 represents a very flexible and C4 represents a very stiff connection.

The two-bar frame is loaded by a horizontal force H as shown in Fig. 20, the load–deflection behavior of the frame using different models and connections are shown in Figs 22–25. Failure of the structure is due to the formation of a plastic hinge at the junction of the beam and column. For Connections C1 and C2, the plastic hinge developed in the

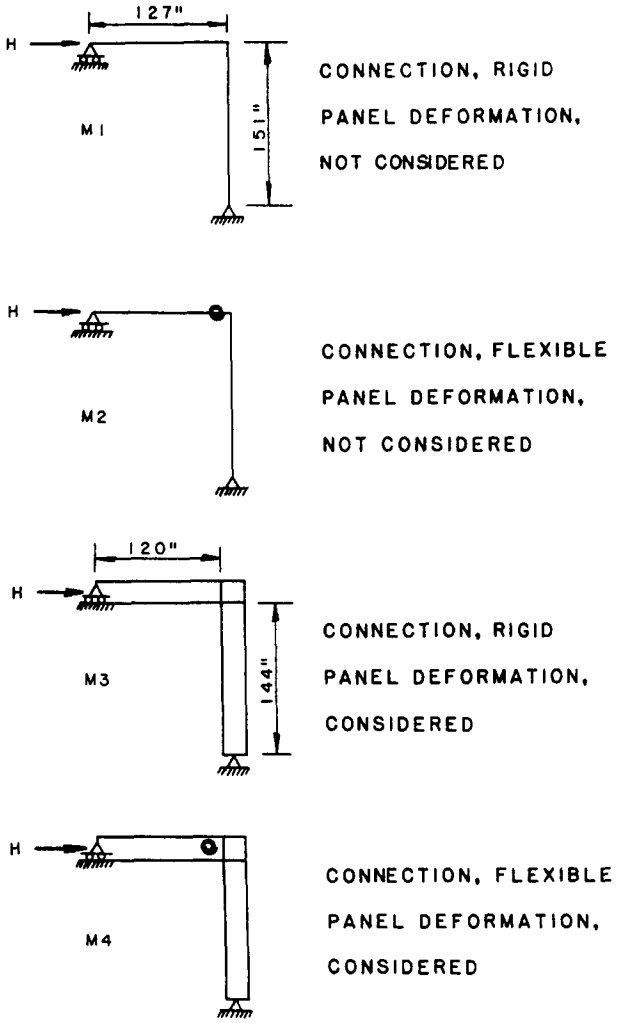

Fig. 20. Structural modeling of a two-bar frame (1 in. = 25.4 mm).

connection when the ultimate capacity of the connection was exhausted. However, for Connections C3 and C4, the plastic hinge developed in the column at the beam and column juncture because the ultimate moment capacities of these two connections exceed the plastic moment capacities of the sections. This explains why the ultimate loads of the subassemblages using Connections C1 and C2 are less than that of the subassemblages using Connections C3 and C4. For C1 and C2, the ultimate load is dictated by the strength of the connections, whereas for C3 and C4, the ultimate load is controlled by the strength of the sections.

If we examine Figs 22–25 carefully, we can conclude that Model 2 will give a satisfactory approximation to Model 4 provided that the connections are relatively flexible when compared to the adjoining beam and column (e.g. C1 and C2). This is because the contribution to additional drift from the flexible connection far outweighs the contribution from panel zone deformation. However, for relatively stiff connections (e.g. C3 and C4), Model 2 and Model 3 will give comparable results which means the contribution to additional drift from panel zone distortion will be as important as that from connection flexibility. As a rough estimate, if $(R_{ki}L/EI) \leqslant 5$, where R_{ki} is the initial stiffness of the connection and L, E and I are respectively the length, elastic modulus and moment of inertia of the member to which the connection is attached, then Model 2 is justified to be used in place of Model 4.

To examine the effect of panel zone deformation on the drift of the frame, the load–deflection behavior of the two-bar frame assuming rigid connection using Model 1 and

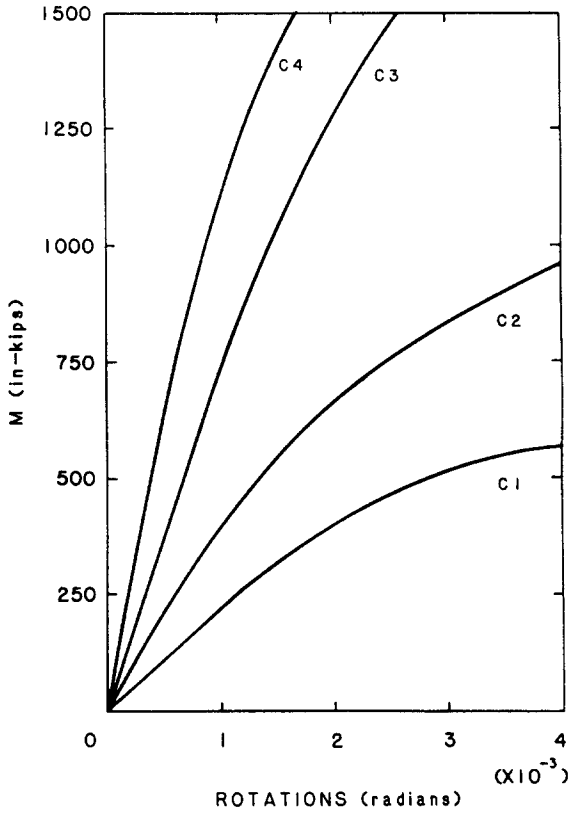

Fig. 21. Connection moment–rotation behavior used for the two-bar frame (1 in.-kip = 113 N-m).

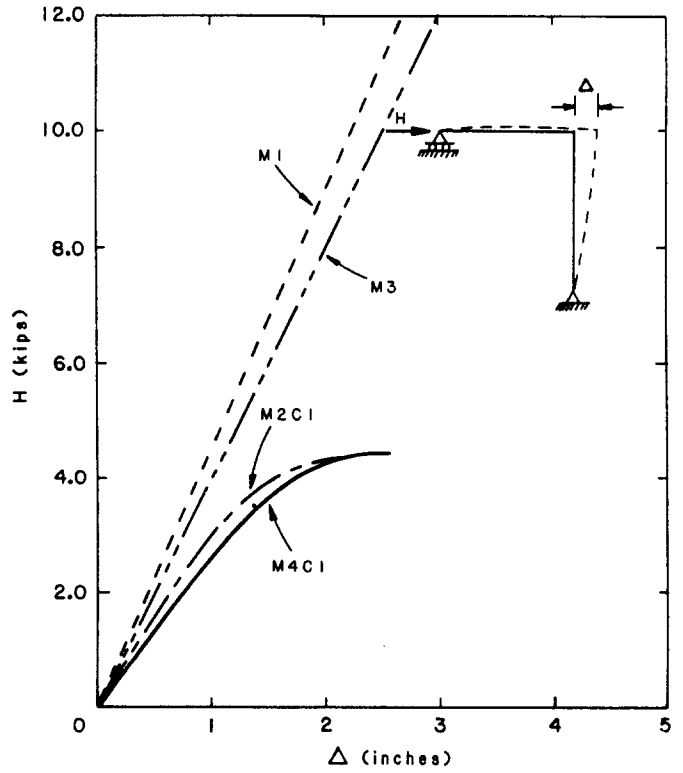

Fig. 22. Load–deflection behavior of the two-bar frame using Connection C1 (1kip = 4.45 kN, 1 in. = 25.4 mm).

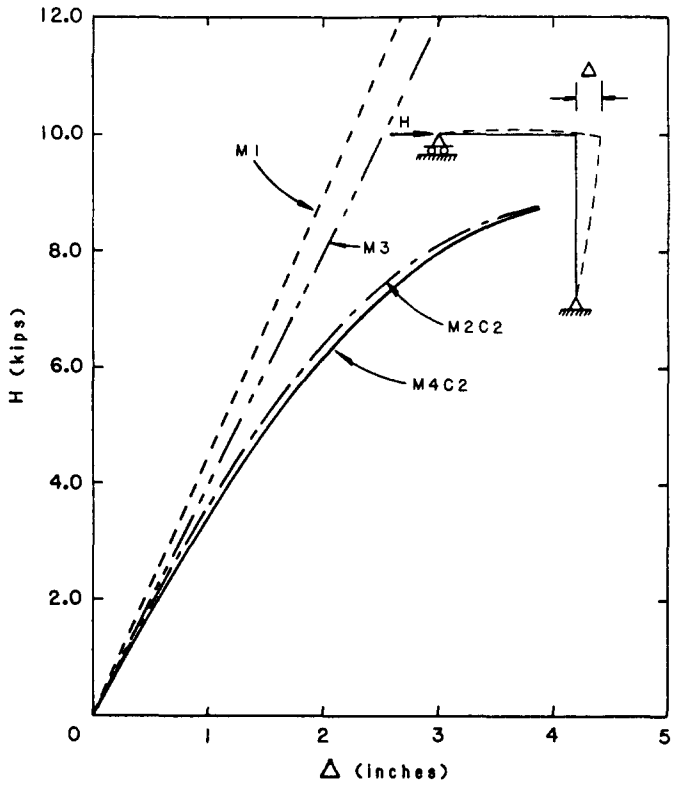

Fig. 23. Load–deflection behavior of the two-bar frame using Connection C2 (1kip = 4.45 kN, 1 in. = 25.4 mm).

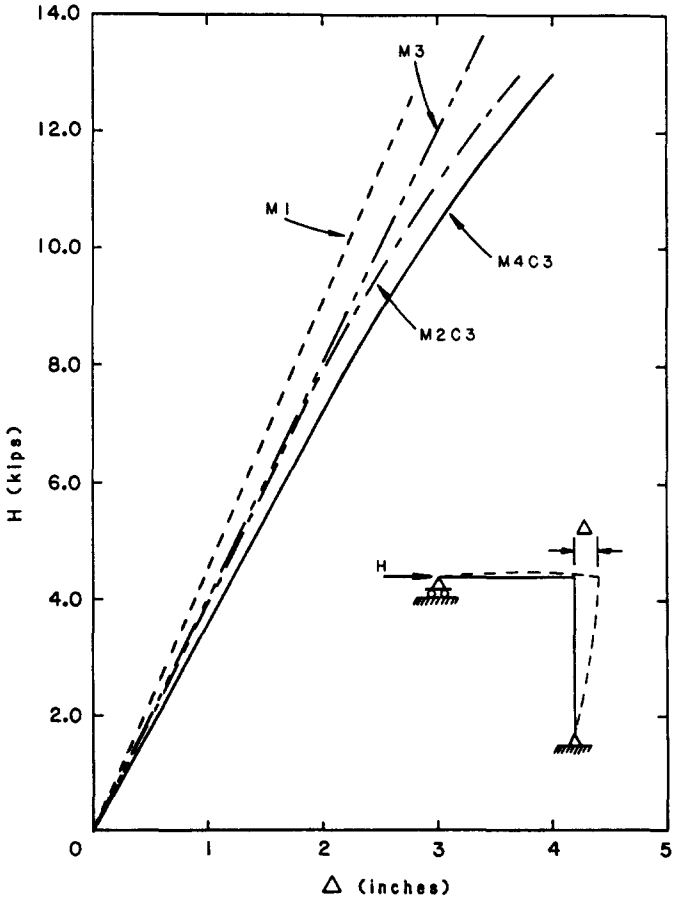

Fig. 24. Load–deflection behavior of the two-bar frame using Connection C3 (1kip = 4.45 kN, 1 in. = 25.4 mm).

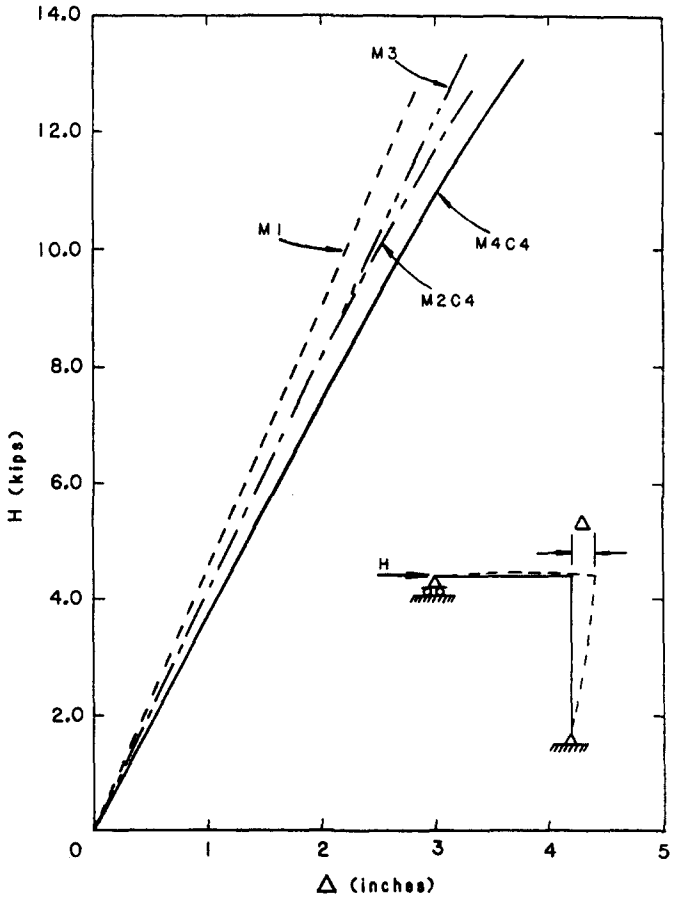

Fig. 25. Load–deflection behavior of the two-bar frame using Connection C4 (1kip = 4.45 kN, 1 in. = 25.4 mm).

Model 3 is shown in Fig. 26. It can be seen that at working load, 13% drift of the frame is due to panel zone deformation. This indicates that panel zone deformation should be considered in the design of moment-resisting frames.

SUMMARY

The behavior of the panel zone is described and a model to represent the panel deformational behavior (extensional, shear, bending) is presented. The validity of the model is shown by comparison with experiments and the importance of the panel zone deformation on the drift of a structure under service load is demonstrated by the analysis of a two-bar frame.

CONCLUSIONS

Experiments on connection subassemblages conducted in the past decade have shown that the panel zone plays an important role in affecting the serviceability and ultimate behavior of moment-resisting frames. Because of the deformational and inelastic behavior of the panel zone, the drift and strength of the frame will be affected. The effects of panel zone deformation and inelasticity are usually undesirable since they will cause an increase in frame drift and a decrease in frame strength. In this paper, a simple model to represent the behavior of the panel zone was described. The implementation of this model in structural analysis was presented. The inclusion of panel zone deformation in frame analysis increases the number of degrees of freedom of the analytical model, yet better prediction of frame behavior can be achieved.

For moment-resisting frames in which connections of high rigidities are used, panel zone deformation is an important factor to be considered in the analysis and design of the frames.

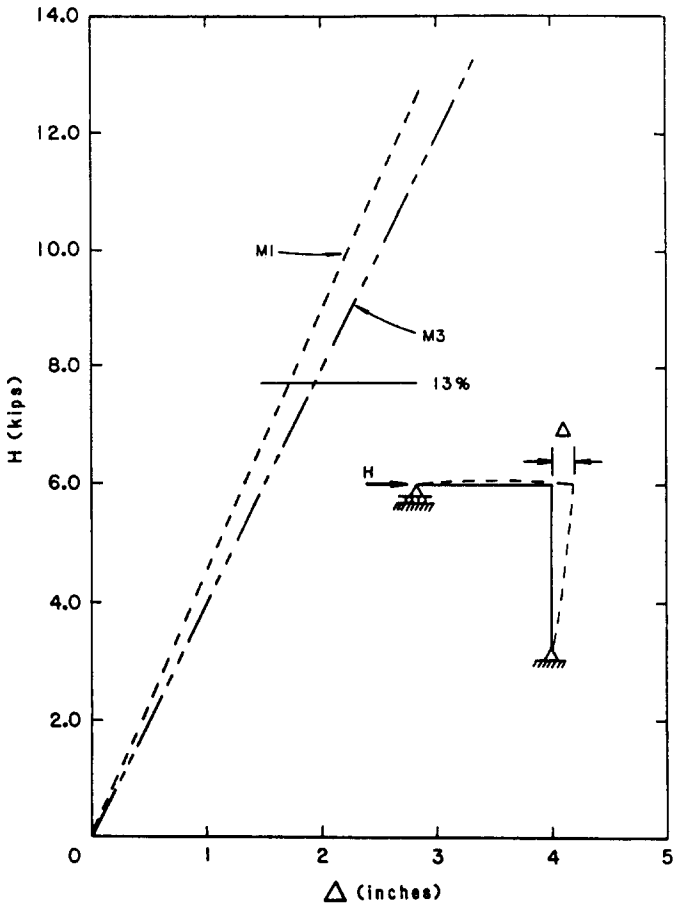

Fig. 26. Effect of panel zone deformation on the drift of the two-bar frame (1 kip = 4.45 kN, 1 in. = 25.4 mm).

REFERENCES

1. R. Becker, Panel zone effect on the strength and stiffness of steel rigid frames. *Eng. J., AISC* **12**, 19–29 (1975).
2. V. V. Bertero, E. P. Popov and H. Krawinkler, Beam-column subassemblages under repeated loading. *J. Struct. Div, Proc. ASCE* **98**, 1137–1159 (1972).
3. W. F. Chen, *Plasticity of Reinforced Concrete*. McGraw-Hill, New York (1982).
4. D. J. Fielding and J. S. Huang, Shear on beam-to-column connections. *Welding J.* **50** (July 1971).
5. D. J. Fielding and W. F. Chen, Steel frame analysis and connection shear deformation, *J. Struct. Div., Proc. ASCE* **99**, 1–18 (1973).
6. B. Kato, Beam-to-column connection research in Japan. *J. Struct. Div., Proc. ASCE* **108**, 343–360 (1982).
7. H. Krawinkler, Shear in beam-column joints in seismic design of steel frames. *Eng. J., AISC* **15**, 82–91 (1978).
8. E. M. Lui, Effects of connection flexibility and panel zone deformation on the behavior of plane steel frames. Thesis presented to Purdue University, West Lafayette, Indiana, in partial fulfillment of the requirements for the Degree of Doctor of Philosophy (1985).

APPENDIX I—KINEMATIC MATRICES

(1) Face 1—Category A

$$\mathbf{T}_{fp} = \begin{bmatrix} 1/2 & 0 & h/12 & 1/2 & 0 & -h/12 \\ t_f/h & 1/2 & t_f/2 & -t_f/h & 1/2 & t_f/2 \\ -1/h & 0 & 0 & 1/h & 0 & 0 \end{bmatrix}$$

(2) Face 1—Category B

$$\mathbf{T}_{fp} = \begin{bmatrix} 1/2 & 0 & h/8 & 1/2 & 0 & -h/8 \\ 3t_f/2h & 1/2 & 3t_f/4 & -3t_f/2h & 1/2 & 3t_f/4 \\ -3/2h & 0 & -1/4 & 3/2h & 0 & -1/4 \end{bmatrix}$$

(3) Face 2

$$\mathbf{T}_{fp} = \begin{bmatrix} 1/2 & 0 & 0 & 1/2 & 0 & 0 \\ 0 & 1/2 & 0 & 0 & 1/2 & 0 \\ 0 & 0 & 1/2 & 0 & 0 & 1/2 \end{bmatrix}$$

(4) Face 3—Category A

$$\mathbf{T}_{fp} = \begin{bmatrix} 1/2 & 0 & -h/12 & 1/2 & 0 & h/12 \\ t_f/h & 1/2 & -t_f/2 & -t_f/h & 1/2 & -t_f/2 \\ 1/h & 0 & 0 & -1/h & 0 & 0 \end{bmatrix}$$

(5) Face 3—Category B

$$\mathbf{T}_{fp} = \begin{bmatrix} 1/2 & 0 & -h/8 & 1/2 & 0 & h/8 \\ 3t_f/2h & 1/2 & -3t_f/4 & -3t_f/2h & 1/2 & -3t_f/4 \\ 3/2h & 0 & -1/4 & -3/2h & 0 & -1/4 \end{bmatrix}$$

(6) Face 4

$$\mathbf{T}_{fp} = \begin{bmatrix} 1/2 & 0 & 0 & 1/2 & 0 & 0 \\ 0 & 1/2 & 0 & 0 & 1/2 & 0 \\ 0 & 0 & 1/2 & 0 & 0 & 1/2 \end{bmatrix}.$$

APPENDIX II—FRAME ELEMENT TANGENT STIFFNESS MATRIX

The frame element tangent stiffness matrix is expressed[8] as:

$$\dot{\mathbf{k}}_f = \mathbf{T}_{cg}^T \dot{\mathbf{k}}_c \mathbf{T}_{cg} + M_A \mathbf{T}_1 + M_B \mathbf{T}_2 + P\mathbf{T}_3$$

where

M_A = bending moment at the Ath of the beam-column
M_B = bending moment at the Bth of the beam-column
P = axial force

$$\mathbf{T}_{cg} = \begin{bmatrix} -s/L_f & c/L_f & 1 & s/L_f & -c/L_f & 0 \\ -s/L_f & c/L_f & 0 & s/L_f & -c/L_f & 1 \\ -c & -s & 0 & c & s & 0 \end{bmatrix}$$

$$\mathbf{T}_1 = \mathbf{T}_2 = \frac{1}{L_f^2} \begin{bmatrix} -2sc & c^2-s^2 & 0 & 2sc & -(c^2-s^2) & 0 \\ & 2cs & 0 & -(c^2-s^2) & -2sc & 0 \\ & & 0 & 0 & 0 & 0 \\ \text{sym} & & & -2sc & c^2-s^2 & 0 \\ & & & & 2sc & 0 \\ & & & & & 0 \end{bmatrix}$$

$$\mathbf{T}_3 = \frac{1}{L_f} \begin{bmatrix} s^2 & -sc & 0 & -sc & sc & 0 \\ & c^2 & 0 & sc & -c^2 & 0 \\ & & 0 & 0 & 0 & 0 \\ \text{sym} & & & s^2 & -sc & 0 \\ & & & & c^2 & 0 \\ & & & & & 0 \end{bmatrix}$$

L_f = chord length of the deformed member
s = $\sin\Theta$
c = $\cos\Theta$
Θ = inclination of the chord of the deformed member

$$\dot{\mathbf{k}}_c = \frac{EI}{L_f} \begin{bmatrix} s_1 & s_2 & 2AL_f(d_1\Theta_A + d_2\Theta_B)/I \\ & s_1 & 2AL_f(d_2\Theta_A + d_1\Theta_B)/I \\ \text{sym} & & A/I \end{bmatrix}$$

$s_1 = 4 + 2\pi^2\rho/15 - [(0.010\rho + 0.543)/(4+\rho) + (0.004\rho + 0.285)/(8.183+\rho)]\rho^2$
$s_2 = 2 - \pi^2\rho/30 + [(0.010\rho + 0.543)/(4+\rho) - (0.004\rho + 0.285)/(8.183+\rho)]\rho^2$

$$d_1 = \frac{\pi^2\rho s_2 - (s_1+s_2)^2(s_2-2)}{8\pi^2\rho(s_1+s_2)}$$

$$d_2 = \frac{-\pi^2\rho s_2 - (s_1+s_2)^2(s_2-2)}{8\pi^2\rho(s_1+s_2)}$$

$$\rho = \frac{PL^2}{\pi^2 EI}$$

Θ_A = rotation of the Ath end of the member with respect to its chord

Θ_B = rotation of the Bth end of the member with respect to its chord.